

Article

A Point-of-Care Testing Device Utilizing Graphene-Enhanced Fiber Optic SPR Sensor for Real-Time Detection of Infectious Pathogens

Shiyu Jiang^{1,2}, Siyu Qian^{1,*}, Shunning Zhu¹, Jinxin Lu¹, Yunxin Hu^{1,2}, Cheng Zhang³, Yikai Geng¹, Xuefeng Chen¹, Ying Guo¹, Zhaoliang Chen³, Jie Pu³, Zhendong Guo³ and Shengchun Liu^{1,*} 

- ¹ Heilongjiang Provincial Key Laboratory of Metamaterials Physics and Device, Heilongjiang University, Harbin 150080, China; jiangshiyv@163.com (S.J.); a1020318309@gmail.com (S.Z.); 18845594580@163.com (J.L.); huyunxinmail@163.com (Y.H.); 18032866837@163.com (Y.G.); chenxuefeng_vip@163.com (X.C.); guoying@hlju.edu.cn (Y.G.)
- ² School of Electronic Engineering, Heilongjiang University, Harbin 150080, China
- ³ Changchun Veterinary Research Institute, Chinese Academy of Agricultural Sciences, Changchun 130122, China; zc1349@foxmail.com (C.Z.); zl981429835@163.com (Z.C.); pujie17765367564@163.com (J.P.); guozd@foxmail.com (Z.G.)
- * Correspondence: qiansiyu@hlju.edu.cn (S.Q.); liushengchun@hlju.edu.cn (S.L.)

Abstract: Timely detection of highly infectious pathogens is essential for preventing and controlling public health risks. However, most traditional testing instruments require multiple tedious steps and ultimately testing in hospitals and third-party laboratories. The sample transfer process significantly prolongs the time to obtain test results. To tackle this aspect, a portable fiber optic surface plasmon resonance (FO-SPR) device was developed for the real-time detection of infectious pathogens. The portable device innovatively integrated a compact FO-SPR sensing component, a signal acquisition and processing system, and an embedded power supply unit. A gold-plated fiber is used as the FO-SPR sensing probe. Compared with traditional SPR sensing systems, the device is smaller size, lighter weight, and higher convenience. To enhance the detection capacity of pathogens, a monolayer graphene was coated on the sensing region of the FO-SPR sensing probe. Severe acute respiratory syndrome coronavirus 2 (SARS-CoV-2) was used to evaluate the performance of the portable device. The device can accurately detect the SARS-CoV-2 spike S1 protein in phosphate-buffered saline (PBS) and artificial saliva within just 20 min, and the device successfully detected cultured SARS-CoV-2 virus. Furthermore, the FO-SPR probe has long-term stability, remaining stable for up to 8 days. It could distinguish between the SARS-CoV-2 spike protein and the MERS-CoV spike protein. Hence, this FO-SPR device provides reliable, rapid, and portable access to test results. It provides a promising point-of-care testing (POCT) tool for on-site screening of infectious pathogens.

Keywords: surface plasmon resonance; infectious pathogen detection; portable device; graphene film; point-of-care testing



Citation: Jiang, S.; Qian, S.; Zhu, S.; Lu, J.; Hu, Y.; Zhang, C.; Geng, Y.; Chen, X.; Guo, Y.; Chen, Z.; et al. A Point-of-Care Testing Device Utilizing Graphene-Enhanced Fiber Optic SPR Sensor for Real-Time Detection of Infectious Pathogens. *Biosensors* **2023**, *13*, 1029. <https://doi.org/10.3390/bios13121029>

Received: 16 November 2023

Revised: 4 December 2023

Accepted: 8 December 2023

Published: 14 December 2023



Copyright: © 2023 by the authors. Licensee MDPI, Basel, Switzerland. This article is an open access article distributed under the terms and conditions of the Creative Commons Attribution (CC BY) license (<https://creativecommons.org/licenses/by/4.0/>).

1. Introduction

Potential pandemic pathogens, such as human influenza A (H5N1) [1], Middle East respiratory syndrome (MERS) [2], severe acute respiratory syndrome (SARS) [3], and severe acute respiratory syndrome coronavirus 2 (SARS-CoV-2) [4] have continued to threaten human health and became the major public health concerns [5]. However, current conventional pathogen detection devices, including cell cultivation, enzyme-linked immunosorbent assay (ELISA), and reverse transcription-polymerase chain reaction (RT-PCR), are usually performed in medical laboratories. They not only need bulky testing equipment but also need professional experimental technologists. These methods suffer from some drawbacks such as long turnaround time, high cost, and complex operations [6].

These limitations make laboratory-based detection nearly impossible for timely on-site inspection [7]. Therefore, developing a portable and user-friendly device for rapid and real-time field detection is necessary.

Point-of-care testing (POCT) is a decentralized detection form of modern laboratory medicine that can be applied directly at the patient's bedside or the screening site [8]. It offers the advantages of rapid acquisition and cost-effectiveness [9]. As a result, rapid and portable diagnostic POCT analysis methods such as test strips are widely used in medicine clinics [10–12]. However, the ability to provide only “yes/no” test results seriously restricts further application in clinical medical diagnosis and quantitative analysis.

As an effective method for label-free real-time medical diagnostics, surface plasmon resonance (SPR) biosensors have proven themselves to be a powerful tool for quantitative pathogen detection [13–15]. Shahriar Mostufa et al. reported a hybrid TiO_2/Au /graphene layer-based SPR sensor with improved sensitivity and capability for cancer detection is presented [16]. Haneul Yoo et al. reported a reusable sensor chip using a ferromagnetic pattern to capture a layer of magnetic particles. The proposed SPR substrate successfully detects the H1N1 influenza virus [17]. Recently, Awadhesh Kumar et al. proposed a silicon nitride-BP-based SPR biosensor for highly sensitive virus SARS-CoV-2 detection [18]. Commercial SPR instruments exhibit topnotch sensitivity capabilities in pathogen detection. Nevertheless, they are usually bulky, optically designed, and mechanically complex, making them unsuitable for portable detection [19]. Fortunately, fiber optic surface plasmon resonance (FO-SPR) sensing has the advantage of smaller size, lower costs, and simpler optical designs [20,21]. Hence, FO-SPR sensors are promising portable tools for the detection of infectious pathogens, which can easily be adapted to POCT [22–24]. In order to further improve the sensitivity of FO-SPR detection to meet the requirements of POCT, the sensing region was coated with monolayer graphene. The graphene's large surface-to-volume ratio remarkably increases the absorption of biomolecules on the sensor [25,26]. Moreover, graphene is biocompatible [27], enabling bio-functionalization. How to use the FO-SPR sensor to build a portable high-sensitivity pathogen POCT device is a more anticipated research issue for scientists.

In this paper, a portable FO-SPR POCT device was developed for real-time detection of highly infectious pathogens. The device integrated the following parts: (I) FO-SPR sensing component; (II) signal acquisition and processing system; (III) embedded power supply unit. The sensing signals are processed and analyzed by a program written on the LabVIEW-based platform to support automated data acquisition and real-time visualization. Since each part requires different power, a variable voltage circuit is used to distribute the supply voltage for the device rationally. FO-SPR sensing probes are used for infectious pathogen detection. In an effort to further improve the sensitivity, the monolayer graphene is coated on the fiber sensing probe. Meanwhile, the selectivity is achieved by immobilizing specific antibodies onto the sensing probe through 1-pyrenebutyric acid N-hydroxysuccinimide ester (PBASE). The integrated FO-SPR device manifests enormous potential in the POCT of highly infectious pathogens.

2. Materials and Methods

2.1. Materials and Reagents

Cu-based monolayer graphene (Precoating PMMA) was bought from XFNANO Materials Tech Co., Ltd. (Nanjing, China). 1-Pyrenebutyric acid N-hydroxysuccinimide ester (PBASE) was bought from Alfa Aesar (Shanghai, China). Methanol, Isopropyl alcohol, Ferric chloride ($\text{FeCl}_3 \cdot 6\text{H}_2\text{O}$), Phosphate-buffered saline (PBS), 11-Mercaptoundecanoic acid (11-MUA), N-hydroxysulfosuccinimide (NHS), 1-(3-dimethylaminopropyl)-3-ethylcarbodiimide hydrochloride (EDC), and bovine serum albumin (BSA) was purchased from Aladdin (Shanghai, China). Artificial saliva was purchased from An Yongbo Technology Co., Ltd. (Xiamen, China). SARS-CoV-2 spike S1 antibody (Cat: 40150-R007), SARS-CoV-2 Spike S1 Protein (Cat: 40591-V08H), and MERS-CoV Spike S1 Protein (Cat: 40069-V08H) were obtained from Sino Biological Inc. (Beijing, China). Deionized water was obtained by using

the ultrapure water production system and autoclaved at 121 °C for 20 min. Other reagents purchased in this study were analytical pure standards if not otherwise specified.

2.2. SARS-CoV-2 Culture and Inactivation

The SARS-CoV-2 virus (BetaCoV/Beijing/IME-BJ05-2020, inactivated by heating at 56 °C for 1 h [28]) was obtained from Changchun Veterinary Research Institute, Chinese Academy of Agricultural Sciences. The inactivated viruses were stored at −80 °C before use.

2.3. Graphene-Based FO-SPR Sensing Probe Fabrication

The FO-SPR sensing probe used multimode fiber (YOFC Co., Ltd., Shanghai, China) with a core diameter of 400 μm and a numerical aperture of 0.37. As previously reported [29], near the end face of the FO-SPR probe, 1 cm of coating and cladding was peeled off as the sensing area. Then, the sensing area was coated with about 50 nm gold using magnetron sputtering (Quorum Q150RSPlus, East Sussex, UK) [30]. To ensure the uniformity of the coating, a unique rotating structure was made to achieve a 360° rotation of the fiber during the sputtering process. To obtain a terminal reflective sensor, a silver layer was formed on the fiber end face using magnetron sputtering technology. The silver layer was protected by encapsulation with epoxy AB adhesive, which can prevent the oxidation of the silver layer.

The graphene film was coated on the sensing region of FO-SPR probe by the wet transfer method (as shown in Figure S1) [31]. First, the PMMA/graphene/Cu film (0.5 × 1 cm) was etched in 1 M FeCl₃ copper etchant for 1 h to etch off the Cu foil. Then, the suspended transparent PMMA/graphene film was washed three times in a deionized water bath for at least 10 min each time to ensure the residual copper etchant was removed. Next, the PMMA/graphene film suspended in deionized water was transferred to the surface of the sensing zone of the probe and dried at room temperature. Next, the probe was heated at 145 °C for 20 min to enhance the adhesion further. Afterward, the PMMA/graphene-coated probe was immersed in acetone overnight to remove the PMMA layer. The graphene-coated probes were cleaned with acetone and isopropyl alcohol and dried under N₂ airflow.

2.4. SARS-CoV-2 Antibody Bio-Functionalization on the FO-SPR Sensing Probes

Figure 1 shows the bio-functionalized process of the monolayer graphene-coated FO-SPR sensing probe. FO-SPR were immersed in 2 mM PBASE in methanol for 1 h at room temperature, and then rinsed using deionized water and drying under N₂ airflow. Then, the sensing probe was immersed in 250 μg/mL SARS-CoV-2 spike S1 antibody in PBS (pH 7.4) for 6 h and then rinsed using deionized water. To reduce the non-specific adsorption, the probes were blocked with 1 mg/mL BSA for 1 h. Finally, the bio-functionalized FO-SPR sensing probe was stored in PBS at 4 °C before use.

In order to demonstrate the higher sensitivity of graphene-coated sensing probes, the traditional 11-MUA-modified sensing probes were used as the control group (refer to Supplementary Materials). The bio-functionalized process is shown in Figure S2. The SARS-CoV-2 spike S1 antibody was immobilized on the sensing probe by 11-MUA to detect the target pathogen.

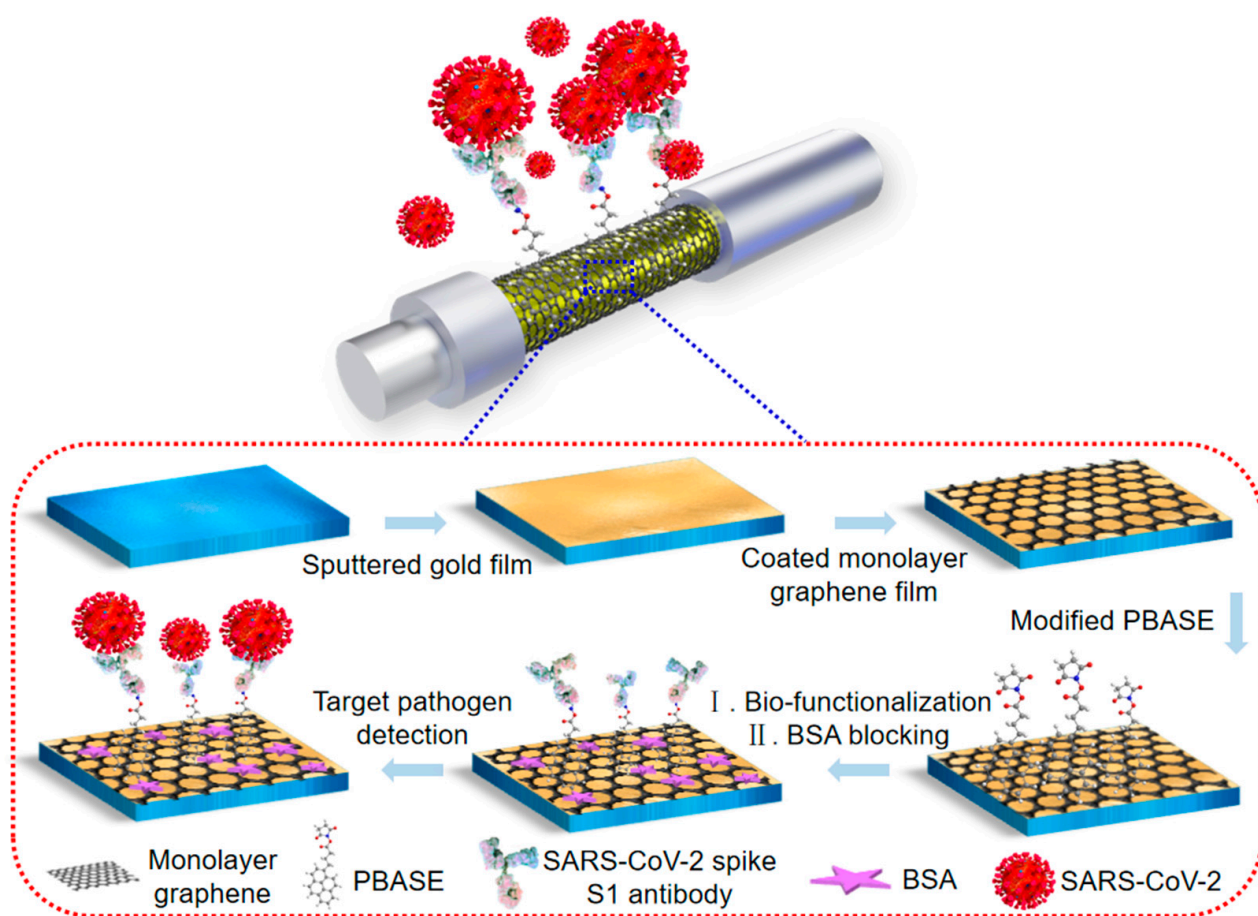


Figure 1. Scheme of the bio-functionalized FO-SPR sensing probe.

2.5. Portable FO-SPR Device Development

The portable FO-SPR device ($250 \times 250 \times 110$ mm) is shown in Figure 2A. Namely, part I (FO-SPR sensing component) consists of a small high-power white LED light source, a miniature spectrometer (Ocean Optic USB2000+, 200–1100 nm), and a bio-functionalized FO-SPR sensing probe (Figure 2B). The sensing probe was connected to the light source and spectrometer via a fiber Y-jumper. For integrated applications, the light source and spectrometer were controlled by the signal acquisition and processing system via USB communication protocol. Part II (signal acquisition and processing system) utilized the self-made LabVIEW program to process and analyze sensor signals from the spectrometer. The program was installed on a microcomputer. The real-time detection data was displayed on a built-in touch screen through the program's user interface, allowing the user to visualize and interpret the results. Moreover, the program controls the current and thus regulates the optical power of the light source. Part III (embedded power supply unit) was used to power the FO-SPR device. To enable outdoor on-site detection, a lithium battery pack with a capacity of 6000 mAh was used for self-powering. The variable voltage circuit was designed to distribute the power supply voltage rationally. Specifically, the lithium battery pack was connected to the input DC 5 V interface of the variable voltage circuit, and it provides three USB ports for outputting voltages of 5 V, 12 V, and 12 V. The 5 V and 12 V ports were connected to the LED light source and the microcomputer for power supply, respectively, and the other 12 V port was linked to the cooling fan. In addition, smartphones via WIFI were used to remotely control the self-made program's operation and transfer test data, as shown in part IV. The device enclosure was designed with a 3D CAD design software (SolidWorks 2021) to mount all functional modules and reduce optical noise from the background light.

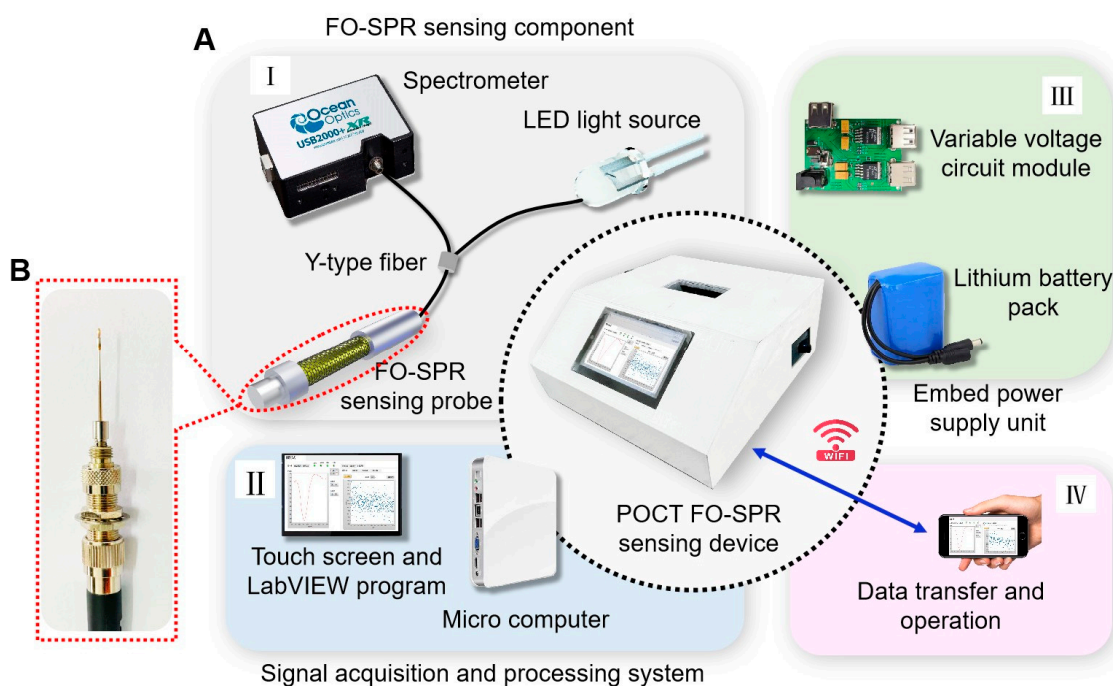


Figure 2. Schematic depiction of the POCT FO-SPR device. (A) Portable FO-SPR optical sensing scheme (I) FO-SPR sensing component. (II) Signal acquisition and processing system. (III) Embedded power supply unit. (IV) WIFI remote control module. (B) FO-SPR sensing probe.

3. Results and Discussion

3.1. Pathogens Detection and Data Analysis

The portable FO-SPR device provided a user-friendly and convenient way to detect the virus in a timely manner. The FO-SPR sensing probe was designed for easy installation and can be conveniently plugged and implemented in the flow cell. SARS-CoV-2 spike protein (10 nM, 20 nM, 35 nM, 45 nM, and 60 nM) and SARS-CoV-2 virus (5×10^3 TCID₅₀/mL, 9×10^3 TCID₅₀/mL, 2×10^4 TCID₅₀/mL, 4×10^4 TCID₅₀/mL and 6×10^4 TCID₅₀/mL) were used as target pathogens. Before testing, PBS was put into the flow cell to achieve the baseline signal of real-time detection. Then, the pathogens were slowly and continuously passed through the flow cell and incubated on the sensing probe for 20 min. Subsequently, the unbound target pathogens were washed off using PBS, a step that caused a slight downward shift in the signal. Next, another concentration of the target pathogen was tested. Repeat the above steps, recording the sensing signals for various analyte concentrations. The limit of detection is determined by the ratio of three times the standard deviation to the sensitivity (S). S is acquired as follows [32]:

$$S = \frac{\lambda - \lambda_0}{C - 0}, \quad (1)$$

where C is the concentration of the tested target pathogen; λ is the response wavelength corresponding to C ; and λ_0 is the wavelength corresponding to blank samples without analytes. The limit of detection (LOD) is calculated as follows [33,34]:

$$LOD = \frac{3\sigma}{S}, \quad (2)$$

where σ is the standard deviation of the test response to the blank sample.

3.2. FO-SPR Sensing Probe Characterization

The monolayer graphene-coated FO-SPR sensing probe is shown in Figure 3. The PBSAE-graphene-modified FO-SPR sensing probe was analyzed by scanning electron mi-

scopy (SEM), Raman spectra, and X-ray photoelectron spectroscopy (XPS). In Figure 3A, SEM shows that the surface of the graphene-coated sensing probe is uniform and pure. To confirm whether successfully modified PBASE on the graphene, the Raman spectrum and XPS are used to analyze the modified FO-SPR sensing surface (Figure 3B–E). The Raman spectra display the PBASE-modified graphene (red) and the pristine graphene (black), as shown in Figure 3B. In the pristine graphene Raman spectrum, there are two major G peaks (roughly at 1580.93 cm^{-1}) and 2D peaks (roughly at 2671.32 cm^{-1}). The G peak is attributed to the lattice vibrations of the sp^2 carbon atoms and the second-order Raman scattering 2D peak [35,36]. After modification with PBASE, there are the D peak (roughly at 1340 cm^{-1}) and D' peak (roughly at 1615 cm^{-1}). They are caused by the resonance modes of the pyrene group in PBASE interacting with the extended phonon modes of graphene [37,38]. In addition, the intensity ratio of graphene characteristic 2D and G peaks (I_{2D}/I_G) decreased from 3.08 (pristine graphene) to 1.24 after PBASE modification. The results indicate the presence of the doping effect on graphene [39]. At the same time, the ratio of I_{2D}/I_G in Raman spectra confirms the monolayer structure of graphene [40]. The 2D peak is shifted to a higher frequency, which is attributed to the doping of graphene by the aromatic molecule PBASE through π - π stacking and tight binding to graphene [41–43]. Thus, the Raman spectra ensure the presence of PBASE on the FO-SPR probe.

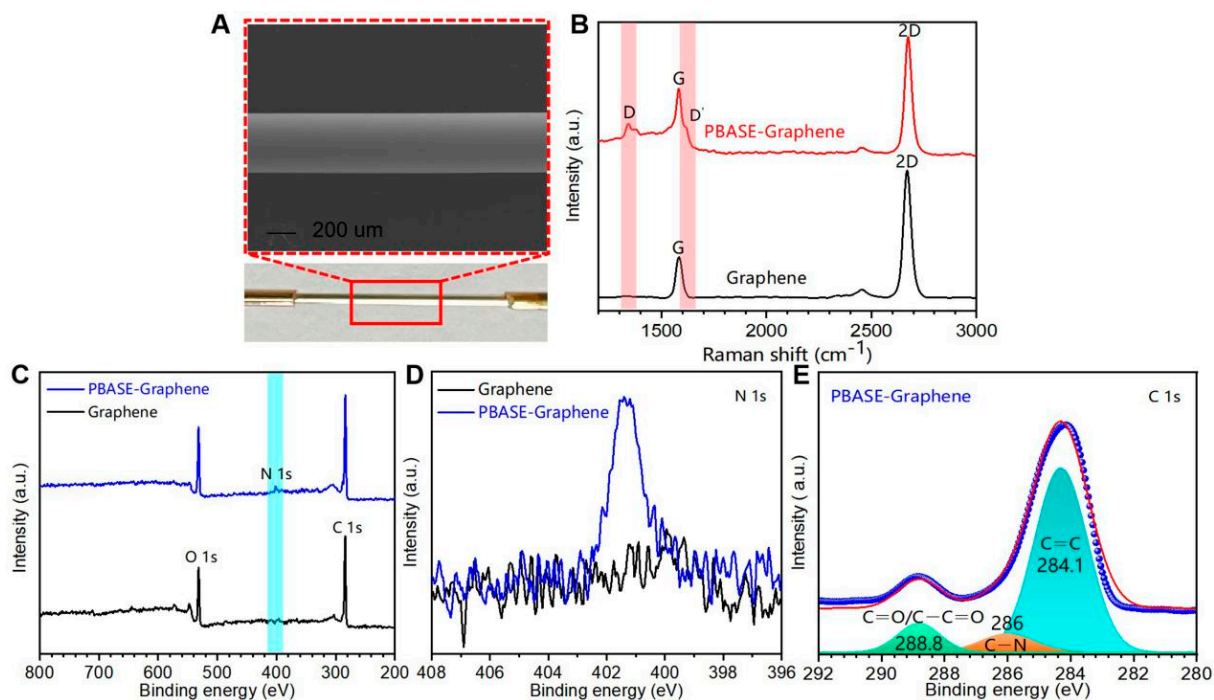


Figure 3. SEM, Raman spectra and XPS of pristine and modified FO-SPR sensing probe. (A) SEM image of modified FO-SPR sensing probe. (B) Raman spectra of pristine graphene (black) and PBASE-modified graphene (red). (C) XPS of pristine graphene (black) and PBASE-modified graphene (blue). (D) XPS N 1s peaks of pristine graphene (black) and PBASE-modified graphene (blue). (E) Deconvolution of PBASE-modified graphene C 1s peaks.

XPS spectroscopy was used to analyze further the presence of PBASE on the graphene-coated FO-SPR sensing surface. Figure 3C shows the XPS spectra of PBASE-modified (blue) and pristine (black) graphene at the C 1s, O 1s, and N 1s peaks. Since the only nitrogen source comes from the PBASE molecule, in Figure 3D, the distinct N1s peak (blue) confirms that PBASE is successfully loaded on the FO-SPR sensing region. In Figure 3E, the C 1s peaks can be deconvoluted into three sub-peaks at around 284.1 eV, 286 eV, and 288.8 eV, which is attributed to the C 1s orbital of C=C, C–N, C=O, and C–C=O, respectively [44]. The peak occurring at 284.1 eV is associated with the C=C aromatic rings

of the sp^2 graphene [45]. The C–N peak appears for the same reason as the N 1 s peak. The C=O/C–C=O is due to the residue of PMMA from the graphene-transferring process [31]. The results provide conclusive evidence that the loading of PBASE-graphene onto the FO-SPR sensing probe was flawless.

3.3. Experimental Verification of FO-SPR Sensing Device Performance

3.3.1. Real-Time Detection of SARS-CoV-2 Spike S1 Protein

To evaluate the performance of the portable FO-SPR device, the SARS-CoV-2 spike protein was detected as the target pathogen. Figure 4A shows a schematic diagram of the antibody-functionalized FO-SPR sensing probe for detecting the SARS-CoV-2 spike protein. PBASE serves as a linker between graphene and antibody. The aromatic pyrenyl group of PBASE binds to the graphene through π – π interaction. Then, the SARS-CoV-2 spike S1 antibody binds with the PBASE through an amidation reaction [46]. In the sensing process, the SARS-CoV-2 spike protein was detected by sensing probes.

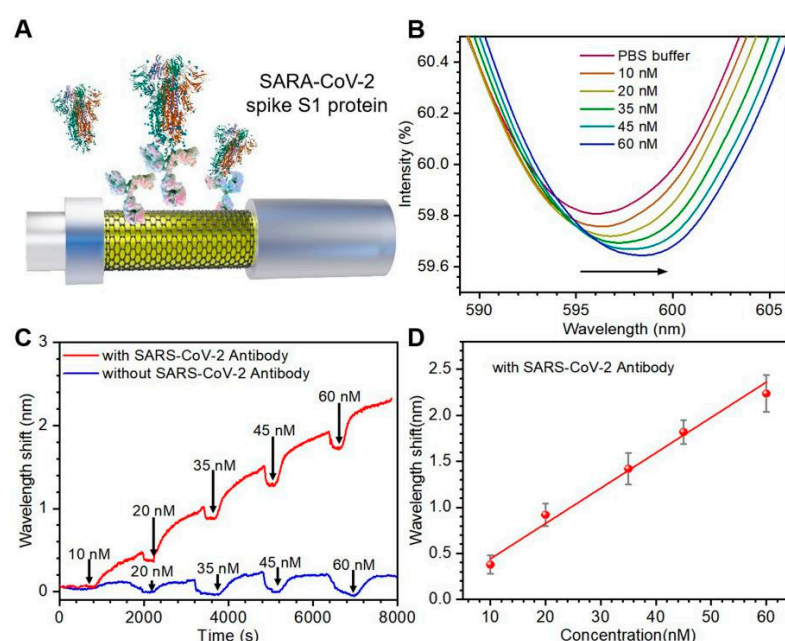


Figure 4. Testing SARS-CoV-2 spike S1 protein by portable FO-SPR device. (A) Schematic diagram of the antibody functionalized sensing probe. (B) SPR spectra of antibody functionalized sensing probes exposed to different concentrations of spike protein (10–60 nM). The arrow indicates the direction of the SPR signal offset. (C) Real-time wavelength shift curves with specific antibodies (red) and without specific antibodies (blue). (D) Linear fit of the maximum wavelength shift with spike protein concentrations. The error bars were determined by the standard deviation of three tests.

Figure 4B shows the SPR spectra curve of different SARS-CoV-2 spike protein concentrations. As the concentration of spike protein increases, the SPR resonance peak drifts toward the long-wave direction. It indicates that more spike protein was bound to the surface of the sensing probe. Figure 4C shows the wavelength real-time shift curve of the SPR spectrum acquired by the self-made program. The FO-SPR sensing probe functionalized with specific antibodies (red) has a significant signal response. By contrast, the sensing probe without functionalized specific antibody shows little noticeable signal responses (blue), and only a small amount of noise fluctuates slightly around the baseline. The experimental results indicate that the sensing probes can effectively prevent non-specific adsorption. In order to confirm whether the wavelength shifts of the SPR spectra can accurately respond to the change of spike protein concentration, a linear fit between the target pathogen concentration C and the maximum intensity shift (λ_{\max}) can be made as shown in Figure 4D. The fitted linear curve is as follows: $\lambda_{\max} = 0.04 \times C + 0.06$ (Correlation

coefficient $R^2 = 0.988$). The LOD is as low as 2.5 nM for spike protein in the linear range of 10–60 nM. The proposed FO-SPR device indicates a good linear relationship, making it suitable for precise analysis and detection of the target pathogen.

To showcase graphene modification can enhance the sensitivity, the FO-SPR sensing probe was coated with graphene and traditional 11-MUA, respectively. Figure S3A shows the wavelength shift of the probe exposed to the spike protein solution. The graphene-coated sensing probe has a higher wavelength shift than the traditional probe. In the linear range (Figure S3B), the LOD of the traditional FO-SPR sensing probe is more than 3-fold lower than that of the graphene-coated probe. The improved sensitivity is caused by the large specific surface area of graphene, which is beneficial for immobilizing more specific antibodies on the sensing surface, enabling more target pathogens to be captured.

For verification of the selectivity, the sensing probes were exposed to 35 nM of MERS-CoV spike protein (control group) and SARS-CoV spike protein (experimental group) sequentially (Figure 5A,B). The SPR spectrum and the real-time signal response curve showed almost no wavelength shift when exposed to the MERS-CoV spike protein. This is ascribed to the absence of interaction between the functionalized sensing probes and the MERS-CoV spike protein. However, the SARS-CoV-2 spike antibody can bind and block the binding epitopes (e.g., receptor binding domains (RBDs) and other related domains on the SARS-CoV-2 spike protein), demonstrating the remarkable response of the SPR spectrum to the SARS-CoV-2 spike antibody. Thus, the portable device shows good selectivity for the target pathogens compared with the control group.

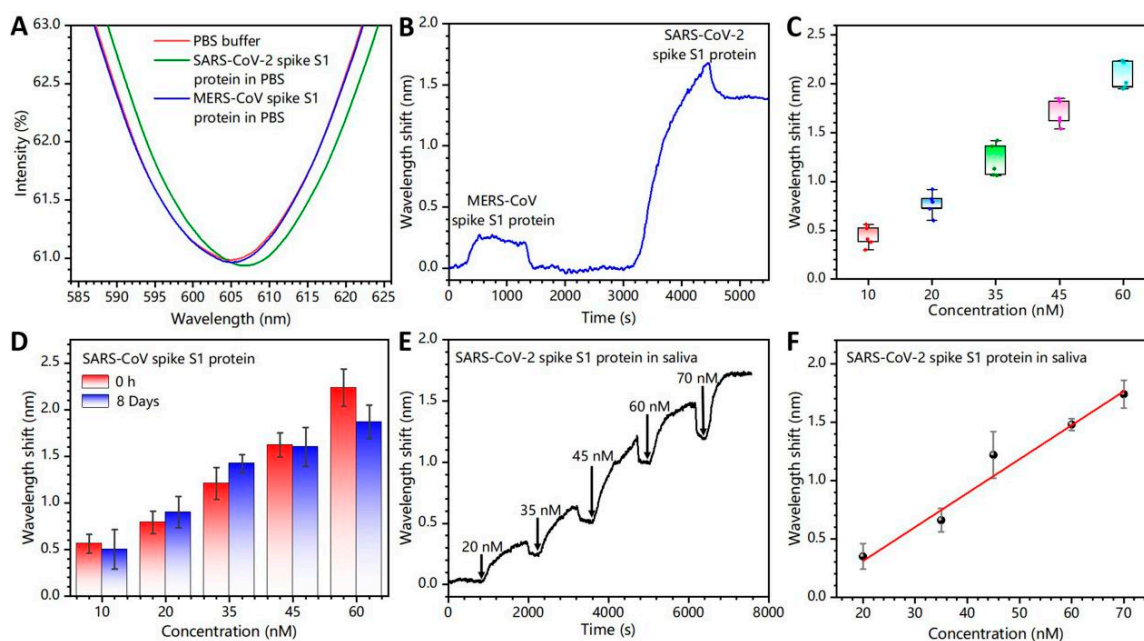


Figure 5. Selectivity testing (A) SPR spectra and (B) real-time response curves for SARS-CoV-2 spike S1 protein and MERS-CoV spike protein. (C) Repeatability test (the error bars were determined by the standard deviation of five tests). (D) Long-term stability tests for FO-SPR sensing probes stored in 4 °C PBS for 0 and 8 days. (E) Real-time response curves for testing of SARS-CoV-2 spike protein in artificial saliva. (F) Linear fit of the maximum wavelength shift with spike protein concentration. The error bars were determined by the standard deviation of three tests.

Repeatability and long-term stability of bio-functionalized FO-SPR devices are also essential parameters. We evaluated the repeatability by testing the SARS-CoV-2 spike protein under identical experimental conditions at various times (Figure 5C). Five measurements were performed on each sample, and the relative standard deviation (*RSD*) was calculated to obtain the device-to-device repeatability, which was denoted as “100%–*RSD*”. The *RSD* is expressed as follows:

$$RSD = \frac{SD}{\bar{X}} \times 100\%, \quad (3)$$

where \bar{X} is the average value of wavelength variation for each experimental group; and SD is the standard deviation. Table S1 shows the repeatability of the device from 77.2–93.2%. Then, the sensing probes were stored in PBS solution at 4 °C for 8 days to verify its long-term stability. Figure 5D shows that the sensing probe still maintains a good detection ability for target pathogens after long-term storage. The results indicate the portable device has stable detection capability and it has promising prospects in clinical application for medical diagnostics.

To evaluate the reliability and accuracy of the FO-SPR device in more realistic situations, the SARS-CoV-2 spike protein was tested in a complex artificial saliva environment. The results demonstrate that the FO-SPR device could successfully detect SARS-CoV-2 spike proteins in saliva (Figure 5E). The LOD was 6.1 nM. Subsequently, a fitted linear curve with R^2 of 0.987 was obtained (Figure 5F). It indicates that the device could avoid interference from other biological components and may be used for highly infectious pathogens content determination and screening.

3.3.2. Real-Time Detection of Inactivated SARS-CoV-2 Virus

Finally, the inactivated SARS-CoV-2 virus was tested via FO-SPR device (Figure 6A). The change of SPR spectra with the concentrations change of SARS-CoV-2 virus (5×10^3 TCID₅₀/mL to 6×10^4 TCID₅₀/mL) are shown in Figure 6B. The sensing probes without specific antibodies were used as negative controls. Figure 6C shows the wavelength shift curve of the sensing probe with specific antibodies (red), exhibiting a significant response compared with the negative control (black). A fitted curve with R^2 of 0.994 was obtained; $\lambda_{\max} = 0.02 \times C^{0.32}$ (Figure 6D). LOD was 2.2×10^3 TCID₅₀/mL. This demonstrates that the FO-SPR device could detect SARS-CoV-2 in real time with high selectivity and has a bright potential application in POCT for highly infectious pathogens.

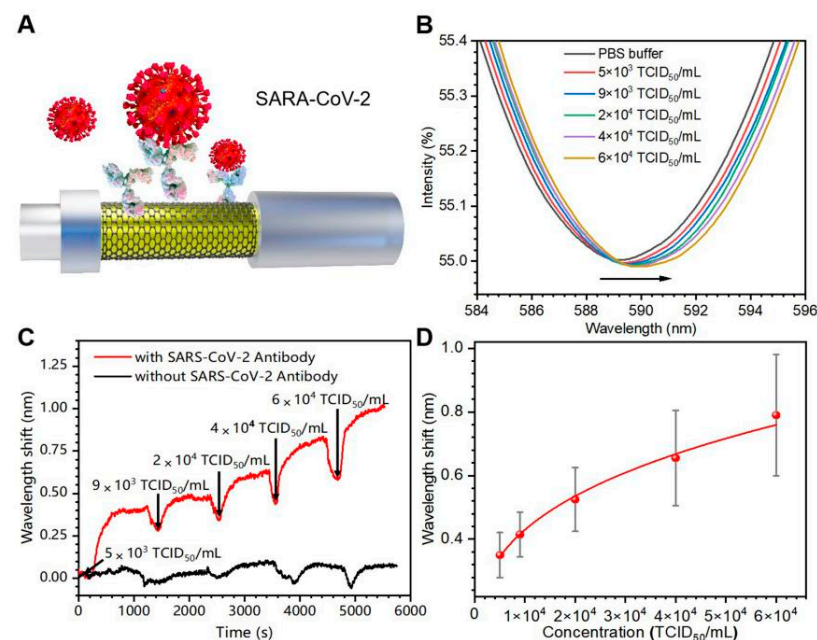


Figure 6. Testing of SARS-CoV-2 inactivated virus in PBS. (A) Schematic diagram of the antibody functionalized FO-SPR sensing probe for detecting SARS-CoV-2 virus. (B) SPR spectra for different SARS-CoV-2 virus concentrations (5×10^3 TCID₅₀/mL to 6×10^4 TCID₅₀/mL). The arrow indicates the direction of the SPR signal offset. (C) Real-time wavelength shift curves with specific antibodies (red) and without specific antibodies (black). (D) Linear fit of the wavelength shifts to different SARS-CoV-2 concentrations. Error bars were determined from the standard deviation of three tests.

4. Conclusions

In conclusion, a portable POCT device has been developed for highly infectious pathogen detection. The device integrates an FO-SPR sensing component, a signal acquisition and processing system, and an embedded power supply unit, all controlled by a self-made program. It offers rapid data visualization for users' timely inspection results. The compact design enhances the convenience of pathogen detection. Moreover, the modification of monolayer graphene contributes to improving the detection sensitivity. The device achieves direct detection of target pathogens without labels within 20 min. For SARS-CoV-2 spike S1 protein detection, LOD is 2.5 nM in PBS and 6.1 nM in artificial saliva. The LOD of the SARS-CoV-2 virus is 2.2×10^3 TCID₅₀/mL. The LOD of the FO-SPR device is similar to other reported SPR biosensors (Table S2). The device exhibits high selectivity for target pathogens, as demonstrated via cross-reactivity experiments with SARS-CoV-2 spike protein and MERS-CoV spike protein. The portable POCT device also presents satisfactory long-term stability (8 days) and repeatability (77.2–93.2%). The above results indicate that the successful development of the portable FO-SPR device provides a reliable technological approach for rapid on-site detection of highly infectious pathogens. This research has great potential to improve the response capacity of infectious disease emergencies and ensure public health security.

Supplementary Materials: The following supporting information can be downloaded at <https://www.mdpi.com/article/10.3390/bios13121029/s1>: Figure S1: Scheme of the graphene-coated FO-SPR sensing probe; Figure S2: Scheme of the bio-functionalized FO-SPR sensing probe; Figure S3: Testing SARS-CoV-2 spike S1 protein by portable FO-SPR device; Table S1: RSD for repeatability analysis; Table S2: Comparison of SPR methods for biosensing analysis [47–54].

Author Contributions: Conceptualization, S.L., S.J. and S.Q.; methodology, S.L., S.J. and S.Q.; software, S.J., S.Z. and J.L.; validation, S.J., S.Z., J.L., Y.H., C.Z. and Y.G. (Yikai Geng); formal analysis, S.J., Y.G. (Ying Guo) and Z.C.; investigation, S.Z., Y.H. and Z.C.; resources, C.Z., Y.G. (Ying Guo), J.P., Z.G. and S.L.; data curation, S.L., S.J. and S.Q.; writing—original draft preparation, S.J., S.L. and S.Q.; writing—review and editing, S.L., S.J., S.Q., X.C., Y.G. (Ying Guo) and Z.G.; visualization, Y.H., X.C. and J.P.; supervision, S.L.; project administration, S.L., S.Q. and X.C.; funding acquisition, S.L., S.Q. and X.C. All authors have read and agreed to the published version of the manuscript.

Funding: This work was funded by the National Natural Science Foundation of China (Nos. 11774081 and 61905069), the Natural Science Foundation of Heilongjiang Province (Nos. TD2021F001, YQ2022F017 and GZ20210029).

Institutional Review Board Statement: Not applicable.

Informed Consent Statement: Not applicable.

Data Availability Statement: Data are contained within the article and Supplementary Materials.

Acknowledgments: The authors express their appreciation to all participants in the study.

Conflicts of Interest: The authors declare no conflict of interest.

References

1. De Jong, M.D.; Simmons, C.P.; Thanh, T.T.; Hien, V.M.; Smith, G.J.D.; Chau, T.N.B.; Hoang, D.M.; Van Vinh Chau, N.; Khanh, T.H.; Dong, V.C.; et al. Fatal outcome of human influenza A (H5N1) is associated with high viral load and hypercytokinemia. *Nat. Med.* **2006**, *12*, 1203–1207. [[CrossRef](#)] [[PubMed](#)]
2. De Wit, E.; van Doremalen, N.; Falzarano, D.; Munster, V.J. SARS and MERS: Recent insights into emerging coronaviruses. *Nat. Rev. Microbiol.* **2016**, *14*, 523–534. [[CrossRef](#)] [[PubMed](#)]
3. Peiris, J.S.M.; Lai, S.T.; Poon, L.L.M.; Guan, Y.; Yam, L.Y.C.; Lim, W.; Nicholls, J.; Yee, W.K.S.; Yan, W.W.; Cheung, M.T. Coronavirus as a possible cause of severe acute respiratory syndrome. *Lancet* **2003**, *361*, 1319–1325. [[CrossRef](#)] [[PubMed](#)]
4. Kevadiya, B.D.; Machhi, J.; Herskovitz, J.; Oleynikov, M.D.; Blomberg, W.R.; Bajwa, N.; Soni, D.; Das, S.; Hasan, M.; Patel, M.; et al. Diagnostics for SARS-CoV-2 infections. *Nat. Mater.* **2021**, *20*, 593–605. [[CrossRef](#)] [[PubMed](#)]
5. Yu, X.; Xia, Y.; Tang, Y.; Zhang, W.L.; Yeh, Y.T.; Lu, H.; Zheng, S.Y. A Nanostructured Microfluidic Immunoassay Platform for Highly Sensitive Infectious Pathogen Detection. *Small* **2017**, *13*, 1700425. [[CrossRef](#)]

6. Wang, C.; Liu, M.; Wang, Z.; Li, S.; Deng, Y.; He, N. Point-of-care diagnostics for infectious diseases: From methods to devices. *Nano Today* **2021**, *37*, 101092. [[CrossRef](#)]
7. Xiao, M.; Tian, F.; Liu, X.; Zhou, Q.; Pan, J.; Luo, Z.; Yang, M.; Yi, C. Virus Detection: From State of the Art Laboratories to Smartphone-Based Point-of-Care Testing. *Adv. Sci.* **2022**, *9*, 2105904. [[CrossRef](#)]
8. Lippa, P.B.; Müller, C.; Schlichtiger, A.; Schlebusch, H. Point-of-care testing (POCT): Current techniques and future perspectives. *TrAC Trends Anal. Chem.* **2011**, *30*, 887–898. [[CrossRef](#)]
9. Liu, J.; Geng, Z.; Fan, Z.; Liu, J.; Chen, H. Point-of-care testing based on smartphone: The current state-of-the-art (2017–2018). *Biosens. Bioelectron.* **2019**, *132*, 17–37. [[CrossRef](#)]
10. Shang, H.; Zhang, X.; Ding, M.; Zhang, A.; Wang, C. Dual-mode paper biosensing platform based on Oxidase-like CoFeMn nanozymes for point-of-care detection of glutathione. *ACS Appl. Nano Mater.* **2023**, *6*, 8907–8915. [[CrossRef](#)]
11. Huang, X.Y.; Chen, L.Z.; Zhi, W.X.; Zeng, R.M.; Ji, G.X.; Cai, H.H.; Xu, J.; Wang, J.Y.; Chen, S.Z.; Tang, Y.; et al. Urchin-Shaped Au–Ag@Pt Sensor Integrated Lateral Flow Immunoassay for multimodal detection and specific discrimination of clinical multiple bacterial infections. *Anal. Chem.* **2023**, *95*, 13101–13112. [[CrossRef](#)] [[PubMed](#)]
12. Sun, F.; Ganguli, A.; Nguyen, J.; Brisbin, R.; Shanmugam, K.; Hirschberg, D.L.; Wheeler, M.B.; Bashir, R.; Nash, D.M.; Cunningham, B.T. Smartphone-based multiplex 30-min nucleic acid test of live virus from nasal swab extract. *Lab Chip* **2020**, *20*, 1621–1627. [[CrossRef](#)] [[PubMed](#)]
13. Gahlaut, S.K.; Pathak, A.; Gupta, B.D.; Singh, J.P. Portable fiber-optic SPR platform for the detection of NS1 antigen for dengue diagnosis. *Biosens. Bioelectron.* **2022**, *196*, 113720. [[CrossRef](#)] [[PubMed](#)]
14. Fathi, F.; Rashidi, M.R.; Omid, Y. Ultra-sensitive detection by metal nanoparticles-mediated enhanced SPR biosensors. *Talanta* **2019**, *192*, 118–127. [[CrossRef](#)] [[PubMed](#)]
15. Dillen, A.; Scarpellini, C.; Daenen, W.; Driesen, S.; Zijlstra, P.; Lammertyn, J. Integrated Signal Amplification on a Fiber Optic SPR Sensor Using Duplexed Aptamers. *ACS Sens.* **2023**, *8*, 811–821. [[CrossRef](#)] [[PubMed](#)]
16. Mostufa, S.; Akib, T.B.A.; Rana, M.M.; Islam, M.R. Highly Sensitive TiO₂/Au/Graphene Layer-Based Surface Plasmon Resonance Biosensor for Cancer Detection. *Biosensors* **2022**, *12*, 603. [[CrossRef](#)] [[PubMed](#)]
17. Yoo, H.; Shin, J.; Sim, J.; Cho, H.; Hong, S. Reusable surface plasmon resonance biosensor chip for the detection of H1N1 influenza virus. *Biosens. Bioelectron.* **2020**, *168*, 112561. [[CrossRef](#)]
18. Kumar, A.; Kumar, A.; Srivastava, S.K. Silicon Nitride-BP-Based Surface Plasmon Resonance Highly Sensitive Biosensor for Virus SARS-CoV-2 Detection. *Plasmonics* **2022**, *17*, 1065–1077. [[CrossRef](#)]
19. Liang, G.; Luo, Z.; Liu, K.; Wang, Y.; Dai, J.; Duan, Y. Fiber Optic Surface Plasmon Resonance-Based Biosensor Technique: Fabrication, Advancement, and Application. *Crit. Rev. Anal. Chem.* **2015**, *46*, 213–223. [[CrossRef](#)]
20. Li, X.; Nguyen, L.V.; Hill, K.; Ebendorff-Heidepriem, H.; Schartner, E.P.; Zhao, Y.; Zhou, X.; Zhang, Y.; Warren-Smith, S.C. All-fiber all-optical quantitative polymerase chain reaction (qPCR). *Sens. Actuators B Chem.* **2020**, *323*, 128681. [[CrossRef](#)]
21. Janik, M.; Hamidi, S.V.; Koba, M.; Perreault, J.; Walsh, R.; Bock, W.J.; Śmietana, M. Real-time isothermal DNA amplification monitoring in picoliter volumes using an optical fiber sensor. *Lab Chip* **2021**, *21*, 397–404. [[CrossRef](#)] [[PubMed](#)]
22. Li, X.; Gong, P.; Zhao, Q.; Zhou, X.; Zhang, Y.; Zhao, Y. Plug-in optical fiber SPR biosensor for lung cancer gene detection with temperature and pH compensation. *Sens. Actuators B Chem.* **2022**, *359*, 131596. [[CrossRef](#)]
23. Peeters, B.; Safdar, S.; Daems, D.; Goos, P.; Spasic, D.; Lammertyn, J. Solid-Phase PCR-Amplified DNase Activity for Real-Time FO-SPR Detection of the MCR-2 Gene. *Anal. Chem.* **2020**, *92*, 10783–10791. [[CrossRef](#)] [[PubMed](#)]
24. Pollet, J.; Delport, F.; Janssen, K.P.F.; Jans, K.; Maes, G.; Pfeiffer, H.; Wevers, M.; Lammertyn, J. Fiber optic SPR biosensing of DNA hybridization and DNA–protein interactions. *Biosens. Bioelectron.* **2009**, *25*, 864–869. [[CrossRef](#)] [[PubMed](#)]
25. Patil, P.O.; Pandey, G.R.; Patil, A.G.; Borse, V.B.; Deshmukh, P.K.; Patil, D.R.; Tade, R.S.; Nangare, S.N.; Khan, Z.G.; Patil, A.M.; et al. Graphene-based nanocomposites for sensitivity enhancement of surface plasmon resonance sensor for biological and chemical sensing: A review. *Biosens. Bioelectron.* **2019**, *139*, 111324. [[CrossRef](#)] [[PubMed](#)]
26. Lu, W.Q.; Yi, Z.; Zhang, J.G.; Xu, X.B.; Tang, B.; Li, G.; Li, G.F.; Zeng, L.C.; Chen, J.; Sun, T.Y. A tunable broadband absorber in the terahertz band based on the proportional structure of a single layer of graphene. *Diam. Relat. Mater.* **2023**, *140*, 110481. [[CrossRef](#)]
27. Morales-Narváez, E.; Baptista-Pires, L.; Zamora-Gálvez, A.; Merkoçi, A. Graphene-based biosensors: Going simple. *Adv. Mater.* **2017**, *29*, 1604905. [[CrossRef](#)]
28. Cui, H.; Zhao, K.; Zhang, C.; Lin, J.; Sun, S.; Li, Q.; Du, L.; Zhang, C.; Liu, J.; Gao, F.; et al. Parapoxvirus-based therapy eliminates SARS-CoV-2 loaded fine aerosol and blocks viral transmission in hamster models. *Front. Microbiol.* **2022**, *13*, 1086627. [[CrossRef](#)]
29. Qian, S.; Chen, X.; Jiang, S.; Pan, Q.; Gao, Y.; Wang, L.; Peng, W.; Liang, S.; Zhu, J.; Liu, S. Direct detection of charge and discharge process in supercapacitor by fiber-optic LSPR sensors. *Nanophotonics* **2020**, *9*, 1071–1079. [[CrossRef](#)]
30. Zhu, Y.Y.; Cheng, J.Y.; Yi, Z.; Tang, B.; Chen, J.; Zhang, J.G.; Xu, X.B.; Tang, C.J.; Sun, T.Y. Spectrally selective solar absorber and thermal infrared suppression based on hollow cylindrical microstructures. *Opt. Commun.* **2023**, *549*, 129910. [[CrossRef](#)]
31. Nguyen, N.H.L.; Kim, S.; Lindemann, G.; Berry, V. COVID-19 Spike Protein Induced Phononic Modification in Antibody Coupled Graphene for Viral Detection Application. *ACS Nano* **2021**, *15*, 11743–11752. [[CrossRef](#)] [[PubMed](#)]
32. He, L.; Yi, Y.T.; Zhang, J.G.; Xu, X.B.; Tang, B.; Li, G.F.; Zeng, L.C.; Chen, J.; Sun, T.Y.; Yi, Z. A four-narrowband terahertz tunable absorber with perfect absorption and high sensitivity. *Mater. Res. Bull.* **2024**, *170*, 112572. [[CrossRef](#)]

33. Qiu, S.; Leng, Y.K.; Yuan, J.H.; Zhang, Z.C.; Zhou, X.; Liu, B.; Mei, C.; Ya, B.B.; Wang, K.R.; Sang, X.Z.; et al. Ultrahigh-sensitivity label-free single mode-tapered multimode-single mode fiber U-shaped biosensor for *Staphylococcus aureus* detection. *Sens. Actuators B Chem.* **2023**, *375*, 132927. [[CrossRef](#)]
34. Karpińska, K.S.; Kudła, P.; Orzeł, U.; Narajczyk, M.; Niedziółka, M.J.; Pałys, B.; Filipek, S.; Ebner, A.; Jönsson, J.N. Investigation of Peptides for Molecular Recognition of C-Reactive Protein-Theoretical and Experimental Studies. *Anal. Chem.* **2023**, *95*, 14475–14483. [[CrossRef](#)] [[PubMed](#)]
35. Soares, R.R.A.; Hjort, R.G.; Pola, C.C.; Parate, K.; Reis, E.L.; Soares, N.F.F.; McLamore, E.S.; Claussen, J.C.; Gomes, C.L. Laser-Induced Graphene Electrochemical Immunosensors for Rapid and Label-Free Monitoring of *Salmonella enterica* in Chicken Broth. *ACS Sens.* **2020**, *5*, 1900–1911. [[CrossRef](#)]
36. Pimenta, M.A.; Dresselhaus, G.; Dresselhaus, M.S.; Cançado, L.G.; Jorio, A.; Saito, R. Studying disorder in graphite-based systems by Raman spectroscopy. *Phys. Chem. Chem. Phys.* **2007**, *9*, 1276–1290. [[CrossRef](#)]
37. Xu, S.; Zhan, J.; Man, B.; Jiang, S.; Yue, W.; Gao, S.; Guo, C.; Liu, H.; Li, Z.; Wang, J.; et al. Real-time reliable determination of binding kinetics of DNA hybridization using a multi-channel graphene biosensor. *Nat. Commun.* **2017**, *8*, 14902. [[CrossRef](#)]
38. Wang, S.; Hossain, M.Z.; Shinozuka, K.; Shimizu, N.; Kitada, S.; Suzuki, T.; Ichige, R.; Kuwana, A.; Kobayashi, H. Graphene field-effect transistor biosensor for detection of biotin with ultrahigh sensitivity and specificity. *Biosens. Bioelectron.* **2020**, *165*, 112363. [[CrossRef](#)]
39. Kwong Hong Tsang, D.; Lieberthal, T.J.; Watts, C.; Dunlop, I.E.; Ramadan, S.; del Rio Hernandez, A.E.; Klein, N. Chemically Functionalised Graphene FET Biosensor for the Label-free Sensing of Exosomes. *Sci. Rep.* **2019**, *9*, 112363. [[CrossRef](#)]
40. Ni, Z.; Wang, H.; Kasim, J.; Fan, H.; Yu, T.; Wu, Y.H.; Feng, Y.; Shen, Z. Graphene thickness determination using reflection and contrast spectroscopy. *Nano Lett.* **2007**, *7*, 2758–2763. [[CrossRef](#)]
41. Wu, G.; Tang, X.; Meyyappan, M.; Lai, K.W.C. Doping effects of surface functionalization on graphene with aromatic molecule and organic solvents. *Appl. Surf. Sci.* **2017**, *425*, 713–721. [[CrossRef](#)]
42. Liu, Y.; Yuan, L.; Yang, M.; Zheng, Y.; Li, L.; Gao, L.; Nerngchamnon, N.; Nai, C.T.; Sangeeth, C.S.S.; Feng, Y.P.; et al. Giant enhancement in vertical conductivity of stacked CVD graphene sheets by self-assembled molecular layers. *Nat. Commun.* **2014**, *5*, 5461. [[CrossRef](#)] [[PubMed](#)]
43. Sun, Y.; Yang, C.; Jiang, X.; Zhang, P.; Chen, S.; Su, F.; Wang, H.; Liu, W.; He, X.; Chen, L.; et al. High-intensity vector signals for detecting SARS-CoV-2 RNA using CRISPR/Cas13a couple with stabilized graphene field-effect transistor. *Biosens. Bioelectron.* **2023**, *222*, 114979. [[CrossRef](#)] [[PubMed](#)]
44. Yang, W.; Jiang, M.; Jiang, S.; Du, L.; Cheng, Y.; Li, P.; Wang, C. Design and fabrication of Gr/Ag-coated tilted grating sensor for ultra-sensitive detection of DNA hybridization. *Sens. Actuators B Chem.* **2022**, *359*, 131587. [[CrossRef](#)]
45. Ang, W.L.; Lim, R.R.X.; Ambrosi, A.; Bonanni, A. Rapid electrochemical detection of COVID-19 genomic sequence with dual-function graphene nanocolloids based biosensor. *FlatChem* **2022**, *32*, 100336. [[CrossRef](#)]
46. Romagnoli, A.; D'Agostino, M.; Pavoni, E.; Ardiccioni, C.; Motta, S.; Crippa, P.; Biagetti, G.; Notarstefano, V.; Rexha, J.; Perta, N.; et al. SARS-CoV-2 multi-variant rapid detector based on graphene transistor functionalized with an engineered dimeric ACE2 receptor. *Nano Today* **2023**, *48*, 101729. [[CrossRef](#)]
47. Xiao, C.Q.; Jiang, F.L.; Zhou, B.; Li, R.; Liu, Y. Immobilization of *Escherichia coli* for detection of phage T4 using surface plasmon resonance. *Sci. China Chem.* **2012**, *55*, 1931–1939. [[CrossRef](#)]
48. Makhneva, E.; Farka, Z.; Skládal, P.; Zajíčková, L. Cyclopropylamine plasma polymer surfaces for label-free SPR and QCM immunosensing of *Salmonella*. *Sens. Actuators B Chem.* **2018**, *276*, 447–455. [[CrossRef](#)]
49. Svärd, A.; Neilands, J.; Palm, E.; Svensäter, G.; Bengtsson, T.; Aili, D. Protein-Functionalized Gold Nanoparticles as Refractometric Nanoplasmonic Sensors for the Detection of Proteolytic Activity of *Porphyromonas gingivalis*. *ACS Appl. Nano Mater.* **2020**, *3*, 9822–9830. [[CrossRef](#)]
50. Inci, F.; Saylan, Y.; Kojouri, A.M.; Ogut, M.G.; Denizli, A.; Demirci, U. A disposable microfluidic-integrated hand-held plasmonic platform for protein detection. *Appl. Mater. Today* **2020**, *18*, 100478. [[CrossRef](#)]
51. Sarcina, L.; Mangiatordi, G.F.; Torricelli, F.; Bollella, P.; Gounani, Z.; Österbacka, R.; Macchia, E.; Torsi, L. Surface Plasmon Resonance Assay for Label-Free and Selective Detection of HIV-1 p24 Protein. *Biosensors* **2021**, *11*, 180. [[CrossRef](#)] [[PubMed](#)]
52. Wang, Q.; Jing, J.Y.; Wang, B.T. Highly Sensitive SPR Biosensor Based on Graphene Oxide and Staphylococcal Protein A Co-Modified TFBG for Human IgG Detection. *IEEE Trans. Instrum. Meas.* **2019**, *68*, 3350–3357. [[CrossRef](#)]
53. Cennamo, N.; Pasquardini, L.; Arcadio, F.; Lunelli, L.; Vanzetti, L.; Carafa, V.; Altucci, L.; Zeni, L. SARS-CoV-2 spike protein detection through a plasmonic D-shaped plastic optical fiber aptasensor. *Talanta* **2021**, *233*, 122532. [[CrossRef](#)] [[PubMed](#)]
54. Qu, J.H.; Ordutowski, H.; Tricht, C.V.; Verbruggen, R.; Gallardo, A.B.; Bulcaen, M.; Ciwinska, M.; Cisneros, C.C.; Devriese, C.; Guluzade, S.; et al. Point-of-care therapeutic drug monitoring of adalimumab by integrating a FO-SPR biosensor in a self-powered microfluidic cartridge. *Biosens. Bioelectron.* **2022**, *206*, 114125. [[CrossRef](#)]

Disclaimer/Publisher's Note: The statements, opinions and data contained in all publications are solely those of the individual author(s) and contributor(s) and not of MDPI and/or the editor(s). MDPI and/or the editor(s) disclaim responsibility for any injury to people or property resulting from any ideas, methods, instructions or products referred to in the content.